Lab on a Chip

COMMUNICATION

View Article Online
View Journal | View Issue

Cite this: *Lab Chip*, 2023, **23**, 2710

Received 28th February 2023,
Accepted 15th May 2023

DOI: 10.1039/d3lc00169e

rsc.li/loc

Room-temperature bonding of glass chips *via* PTFE-assisted plasma modification for nanofluidic applications†

Qiushi Kang,[a] Chenxi Wang, *[a] Kaimeng Liu[a] and Takehiko Kitamori [b]

Fused-silica glass, as a desirable material with rigidity, biological inertness, and favorable light transmission for nanofluidic devices, should be assembled *via* low-temperature bonding technology to hermetically seal channels for stable liquid manipulation in extended-nano (10^1–10^3 nm) space. Confronted with the predicament of localized functionalization of nanofluidic applications (*e.g.* DNA microarray) with temperature-sensitive structures, the room-temperature direct bonding of glass chips to achieve modification of channels prior to bonding offers a considerably attractive solution to avoid component denaturation during the conventional post-bonding heating process. Therefore, we developed a nano-structure friendly and technically convenient room-temperature (RT, 25 °C) glass–glass direct bonding technology using polytetrafluoroethylene (PTFE)-assisted plasma modification without a requirement for special equipment. Unlike the establishment of chemical functionalities relying on immersion in potent but dangerous chemicals like HF, the fluorine radicals (F*) from PTFE pieces with superior chemical inertness were introduced on glass surfaces *via* O_2 plasma sputtering and constructed fluorinated silicon oxides on the glass surfaces effectively, eliminating the significant etching effect of HF to protect fine nanostructures. Very strong bonding was obtained at RT with no heating and the high-pressure resistant glass–glass interfaces were evaluated under high-pressure-driven flow conditions up to 2 MPa based on a two-channel liquid introduction system. Moreover, the favorable optical transmittance of the fluorinated bonding interface demonstrated a capacity for high-resolution optical detection or liquid sensing.

1. Introduction

The concept of lab-on-a-chip aims to integrate the capability of a laboratory into a miniaturized nanofluidic system for rapid and accurate detection at the chip scale which is close to commercial reality. Owing to the manipulation of liquid-containing reagents at an extended nanoscale (typically 10^1–10^3 nm) to control reactions, nanofluidics has attracted much attention for its promising applications using its dominant surface effect and extremely small volume, spanning disease monitoring and management, chemical synthesis, biomedical tissue engineering, and environmental sampling.[1–5] Compared with well-established polymer substrates (*e.g.* polydimethylsiloxane, PDMS) with low stiffness and water permeability, fused-silica glass substrates are extensively used for nanofluidic devices because they offer overwhelming advantages including chemical inertness, higher values of Young's modulus and light transmission, and can be used to fabricate nanostructures with high resolution and avoid fluid leaching and evaporation.[6,7] To achieve nanofluidic devices successfully, it is paramount to construct and hermetically seal channels *via* assembling glass substrates with nanostructures. To date, low-temperature bonding has provided a desirable assembly solution with the merits of protecting high-temperature sensitive functional components immobilized in channels such as biomolecules, electrodes, sensors, waveguides, optical components, *etc.*[8] Adhesive bonding (intermediate-layer bonding), as an important bonding technology performed at low temperatures, can integrate polymer, semiconductor, metal, and ceramic substrates by introducing micron-thick thermal or photo-curable resin at the interface. Seamless, void-free robust glass bonding interfaces have been obtained through PDMS,[9,10] SU-8,[11] and benzocyclobutene (BCB)[12,13] within 300 °C. However, the dispensing of adhesive resin has potential for channel contamination and clogging, and adhesive bonds are not

[a] *State Key Laboratory of Advanced Welding and Joining, Harbin Institute of Technology, Harbin 150001, China. E-mail: wangchenxi@hit.edu.cn*
[b] *Collaborative Research Organization for Micro and Nano Multifunctional Devices, The University of Tokyo, 7-3-1 Hongo, Bunkyo, Tokyo 113-8656, Japan*

† Electronic supplementary information (ESI) available: The characterization of bonding efficiency with different relative humidities, and room temperature bonding energy of glass–glass as a function of storage time in ambient air. The XPS compositional depth analysis of the glass surface activated *via* (O_2 + F*) plasma. Schematic of five positions on the fused-silica glass surface for the XPS measurements and the atomic concentrations (at%) of fluorine at the corresponding positions after (O_2 + F*) plasma treatment for 40 s. The evaluation of bondability of (O_2 + F*) plasma activated surfaces with different air exposure times before bonding at RH = 75% in the atmosphere. See DOI: https://doi.org/10.1039/d3lc00169e

stable enough for long-term service due to the chemical reactivity of resins.

As a clogging-free solution for nanofluidic applications, a direct bonding approach flourishes, relying on low-temperature chemical reactions between functionalized surfaces to achieve covalent bonds eventually, also known as "chemical gluing".[14] Rather than the use of micron-scale resins, liquid chemical "glues" (*e.g.*, 3-aminopropyl trimethoxysilane, APTES) as crosslinking agents can establish a nanometer-scale self-assembled monolayer (SAM) on the surface through several-hours immersion, reducing the risk of channel clogging and interfacial instability.[15,16] It has been reported that C–C or Si–O–Si bonds can be achieved at 150–200 °C between hydroxylated, aminosilylated, or carboxylated glass surfaces according to reactions like the Diels–Alder cycloaddition reaction.[17–19] With ultra-high surface-area-to-volume ratios and ultrashort diffusion lengths, the sealed nanochannels provide a remarkable arena for affinity-based recognition events such as immunoassays or DNA analysis. However, in the case of direct bonding at low temperatures, the immobilization of temperature-sensitive biomolecules should be performed after the bonding process to protect from any possible denaturation (*e.g.* proteins denature at temperatures above 40 °C (ref. 20)). The DNA microarray technique has flourished over the past few years since the partial modifications of nanochannels with DNA ligands with functionality and specificity enable more data to be collected than single-point experiments.[21] In this occasion, however, the bottleneck lies in the formation of covalent bonds at predetermined spots to immobilize different ligands only to portions of the channel, which is difficult to achieve after bonding due to the limited extended nanospace. In order to solve this technical issue, the room-temperature direct bonding of glass chips to realize partial functionalization of channels prior to bonding offers a considerably attractive solution.

To date, the realization of room-temperature bonding essentially relied on surface modification *via* dry or wet approaches. Regarding surface dry activation, wafer-level glass–glass bonding was achieved at room temperature successfully *via* reactive ion etching (RIE) O_2 plasma followed by N_2 radical microwave (MW) plasma activation in the same chamber (so-called sequential plasma activation).[22] Similarly, Takeuchi and co-workers obtained a glass–glass interface with a bonding energy of 1.32 J m^{-2} by means of Ar ion bombardment under ultrahigh vacuum ($<10^{-5}$ Pa) conditions, cooperating with *in situ* AlO film deposition on the glass surfaces.[23] However, owing to the necessity for special activation equipment, the productivity of nanofluidic applications based on the above methods has been greatly limited. In contrast, room-temperature bonding based on surface wet chemical cleaning broke the dilemma about special equipment. For instance, glass–glass interfaces could be attained through room-temperature treatment with sulfuric acid (H_2SO_4),[24] hydrofluoric acid (HF),[25] or hydrogen fluoride steam.[26] Nevertheless, the extensive utilization of dangerous chemicals was not conducive to establishing a toxic-free environment and should be avoided for non-essential societal use. Furthermore, the essence of HF activation lies in the sufficient SiO_2 etching rate (10 nm min^{-1}) based on the chemical reaction ($SiO_2 + 4HF \rightarrow SiF_4\uparrow + 2H_2O$), which could destroy the fine nanostructures in the devices.[25] Recently, a water-droplet bonding method was developed to realize room-temperature glass bonding *via* H_2O as the bonding agent.[6] A pressure endurance of more than 600 kPa within 6 h of bonding was sufficient for cell cultivation, but far from suitable for high-pressure nanofluidic scenarios. Overall, these methods are not cost-effective, nano-structure friendly, or robust enough for the mass production of glass nanofluidics.

Polytetrafluoroethylene (PTFE), also termed Teflon, is generally not suitable as a bonding agent due to its superior chemical inertness under the harshest conditions below 300 °C.[27,28] Notwithstanding, we proposed a technically convenient PTFE-assisted plasma modification strategy *via* commercialized reactive ion etching equipment to construct fluorinated glass surfaces for room-temperature (RT, 25 °C) direct bonding in this work. Different from the significant etching effect of HF, the fluorine radicals (F*) from PTFE pieces were introduced on the glass surface *via* O_2 plasma sputtering and partially replaced Si–O groups with Si–F groups within 40 s, which was considered to be friendly to fine nanostructures. The RT bonding mechanisms were analyzed based on X-ray photoelectron spectroscopy (XPS) and chemical affinity results, and the leak-free glass–glass interface with high bonding energy was examined *via* leakage tests under high-pressure nanofluidic conditions (2 MPa). In addition, the light transmittance of the bulk glass substrate and across the bonding interface was also evaluated, demonstrating the capacity for sensing and diagnostics.

2. Experimental section

2.1 PTFE-assisted surface modification process

Fused-silica glass substrates (70 mm × 30 mm × 0.7 mm) without nanochannels were used in this study to investigate the possibility of room-temperature bonding. Firstly, the glass substrates were immersed in piranha solution (H_2SO_4 : H_2O_2 = 3 : 1) for 8 min to remove organic contaminants effectively. Subsequently, the contamination-free glass substrates were ultrasonically cleaned with deionized water for 5 min and dried *via* a nitrogen flow. To modify the glass substrates with PTFE, the clean glass substrates were placed in the center of a plasma activation chamber side by side while introducing a square frame-shaped PTFE substrate (5 mm thick, 2.18 g cm^{-3}) to surround the glass substrates simultaneously, as shown in Fig. 1. O_2 gas was introduced into the chamber at a pressure of 60 Pa, and the plasma was generated with a discharge power of 200 W at a frequency of 13.56 MHz. Due to the activation and sputtering effect of plasma on glass and PTFE, the glass surfaces can be functionalized *via* treatment for 40 s, and the F concentrations on the glass surface can be controlled by

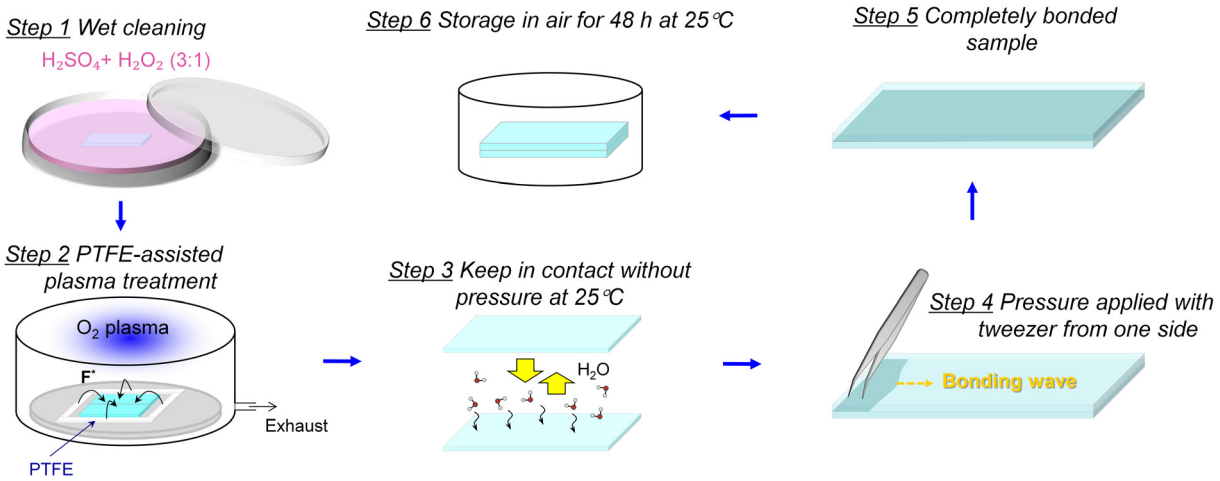

Fig. 1 Schematic drawing of room-temperature bonding of glass chips *via* fluorinated plasma introduced by PTFE.

adjusting the area of the PTFE frame during plasma activation. After the surface activation, two glass substrates were exposed in a storage chamber to achieve subsequent bonding within 30 s, which could control the relative humidity (RH) to terminate the glass surfaces with sufficient H_2O molecules. Owing to the H_2O molecules playing an important role in bridging the microgaps between the surfaces, Fig. S1(a)† displays the bonding area ratio as a function of relative humidity. The effective bonding area was estimated using Photoshop software and was compared with the total bonding area of glass–glass chips. It can be noticed that the bonding area ratio exceeded 95% stably when the RH was more than 75%. The lack of H_2O molecules could barrier the formation of hydrogen networks between the surfaces. Herein, the optimal relative humidity of the storage chamber was 75%. When the glass surfaces were brought into contact, slight pressure was applied from one side of the chip with a tweezer to generate a bonding wave. Once the bonding wave started propagating across the interface, there was no requirement for pressure and a completely bonded interface would be obtained spontaneously. To further stabilize the interface, the glass–glass pairs should be stored at room temperature for 48 h, and the bonding strength and feasibility for nanofluidic devices were subsequently further evaluated. Considering the possible condensation reactions at the interface, the bonded samples were all positioned in a ventilated place such as a ventilating cabinet to facilitate the timely release of trace gaseous by-products.

2.2 Evaluation of bonding energy

To assess the bonding energy, the crack propagation length was recorded to calculate the bonding energy *via* the crack-opening method.[29] This is the most convenient method to measure the strength of bonded samples. A razor with a thickness of t_b (100 μm in this work) was inserted into the bonding interface. The bonding energy (γ) can be obtained *via* the following equation:

$$\gamma = \frac{3t_b^2 E t_w^3}{32L^4}$$

where E is the Young's modulus for the fused silica substrate (6.6×10^{10} Pa), t_w is the glass substrate thickness (7×10^{-4} m), and L is the crack propagation length.

2.3 Leakage test

Chips with two sets of microchannels bridged with 20 parallel nanochannels were fabricated on glass substrates for leakage tests, which is a standard micro/nano hybrid fluidic circuit for liquid manipulation in nanofluidic applications. In this micro/nanohybrid system, the microchannels facilitated the entry and regulation of liquids as well as the external connection on demand, while the nanochannels were employed for subsequent measurement. This nano-in-microfluidic system has distinctive advantages of steady liquid introduction, effective liquid exchange, and prevention of bubbles or dust entering the nanochannels. Therefore, the nano-in-microfluidic system is applicable not only for DNA/RNA analysis,[21,30] but also for streaming potential/current measurement[31] or *in situ* electrokinetic probing[32] for the investigation of extended-nanospace chemistry, as an electrochemical reactor for enzymatic reactions[33,34] to enhance reaction rates, the accurate active regulation of femtoliter-scale fluid flow,[35] *etc.* To be precise, the nanochannels were patterned on one side of the substrate by electron beam lithography, and two sets of microchannels were formed by photolithography on the other substrate, both of which were then subjected to plasma dry etching. Moreover, inlet/outlet holes at the end of microchannels were also drilled. The patterned glass substrates integrated by the abovementioned PTFE-assisted modification were ready to undergo leakage tests. Herein, we designed and developed a two-channel high-pressure liquid introduction system instead of a common air controller to inject sample solutions into the micro and nanochannels under a wide pressure range (50

kPa–2 MPa), which will be illustrated in detail later. By pressure switching and blocking one of the inlet holes of a microchannel, a fluorescent sample solution would be pressurized into nanochannels and another microchannel. Eventually, the channels filled with sample solution and leakage at the bonding interface could be checked on a nanometer-scale level using fluorescence microscopy. Considering the adsorption of fluorescent solution on the glass walls, sulforhodamine B (10 μmoL L^{-1}) was chosen as the fluorescent dye and introduced into the microchannel to avoid interference results and ensure repeatability.

3. Results and discussion

In order to elucidate the effect of PTFE-assisted modification, the chemical state of the glass substrates before and after activations was analyzed by X-ray photoelectron spectroscopy (XPS) first. As displayed in Fig. 2(a), the symmetric peak at 103.9 eV in the Si 2p spectrum of the pristine glass substrate was assigned to Si–O bonds.[36] When the glass substrate was treated only with O_2 plasma without a PTFE frame, the Si–O peak position shifted to a higher binding energy. This shift can be attributed to organic contaminant desorption on the pristine surface *via* chemical bond (*e.g.* C–Si–O) breakage. After O_2 plasma activation, the contaminants decomposed into CO_2 and H_2O, and more Si–O dangling bonds were exposed owing to reactive oxygen radicals (ROS). Concurrently, Fig. 2(b) shows that there were no F-related signals detected on the O_2 plasma-activated glass surface. However, a F signal emerged on the PTFE-assisted activated surface at 685.2 eV which was attributed to Si–F bonds.[37] Due to the sputtering effect of ions with kinetic energy and the reactivity of ROS generated in O_2 plasma, the C–F bonds of the PTFE were broken through chemical oxidation to form CO, CF_xO_y, and most importantly, fluorine radicals (F*), as shown in reaction (1).[28,38] The gaseous CO and CF_x-O_y could desorb from the PTFE surface, while neutral F* could diffuse onto the glass surface. These small amounts of reactive F* would not cause extensive bond breakage but partially broke Si–O bonds to terminate the glass surface with Si–F following exothermic reaction.[39] Given that the essence of PTFE-assisted modification is the introduction of F*, this functionalization can also be denoted as (O_2 + F*) plasma activation.

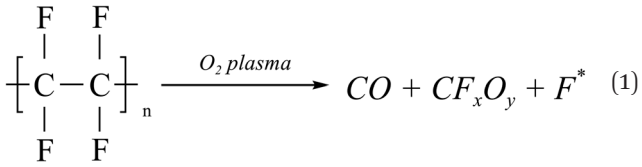

(1)

In addition, XPS compositional depth analysis was also carried out using an Ar-ion beam at an incident angle of 35°, as presented in Fig. S2.† As the surface was etched, it turns out that the F signal was still detectable down to a depth of ~2 nm, suggesting the formation of fluorinated silicon oxide (SiO_xF_y) on the subsurface. To assess the uniformity of the fluorinated silicon oxide, the relative atomic concentration (atomic percentage, at%) of F could be quantitatively characterized and calculated *via* XPS on different positions of the glass surface, including the corner and center parts. As shown in Fig. S3(a),† the fluorine concentrations at five positions of the glass surfaces were analyzed. The relative atomic concentration of fluorine was calculated from the ratio of the fluorine peak areas to the total peak areas in the XPS measurements. It turns out that the concentration of fluorine at the center was slightly lower than at the corners due to the sputtering-like process using peripheral PTFE as the fluorine source, as displayed in Fig. S3(b).† The average fluorine concentration (at%) was 5.522%, demonstrating the formation of a fluorinated oxide layer over the entire 30 mm × 70 mm glass surface.

Albeit a fluorinated glass surface has been formed *via* (O_2 + F*) plasma activation due to the assistance of PTFE, the surface morphology is an important factor that represents the real contact area between the surfaces to assess whether bonding can occur at room temperature. Evaluation of surface roughness in terms of root-mean-square (RMS) values and three-dimensional morphology analysis was achieved by atomic force microscopy (AFM). According to the reduced RMS values (<0.15 nm) shown in Fig. 3(a), it is indicated that

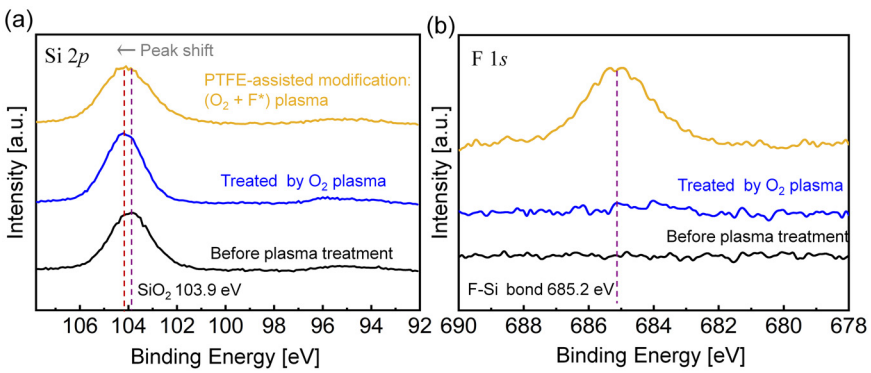

Fig. 2 XPS (a) Si 2p and (b) F 1s core level spectra of glass substrates before and after activations.

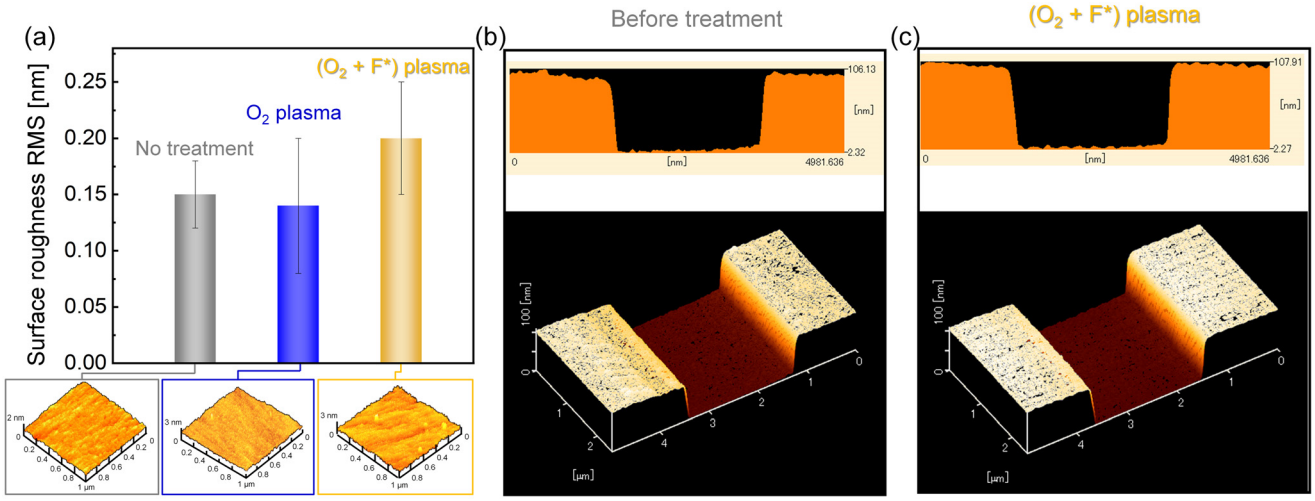

Fig. 3 (a) Surface roughness and topography of glass substrates before and after different activations. AFM images of a shallow nanochannel before and after (O_2 + F*) activation are shown in (b) and (c), respectively.

the glass surface was slightly flattened after O_2 plasma activation due to the desorption of contaminants. In contrast, the glass surface was roughened with the addition of F* in O_2 plasma, and the average RMS value increased to 0.2 nm, even exceeding that of the bare glass surface. Since fluorine-containing gas plays an important role in the etching of SiO_2 during semiconductor fabrication in industry, the slightly rougher glass surface obtained *via* (O_2 + F*) plasma can be attributed to the etching effect of F*. Due to the low concentration of F* radicals, however, the surface morphology has not deteriorated further, and was still smooth enough (<0.5 nm) and conducive to room-temperature bonding. Moreover, AFM 3D images of glass substrates fabricated with nanochannels (100 nm in depth, 2 μm in width) before and after (O_2 + F*) plasma activation are also displayed in Fig. 3(b) and (c). It can be observed that there is little change in the morphology of the nanochannels after (O_2 + F*) plasma activation, indicating that the low concentration of F* will not damage the precise nanostructures on the glass substrate. Therefore, due to the cleaning effect of ROS and the etching action of F*, (O_2 + F*) plasma currently appears to be a viable candidate for bonding glass substrates with complex nanostructures.

Though Si–F groups have been established on the smooth glass surface, the resultant surface energy ought to be further appraised for the correlation between the surface energy and bonding difficulty. According to the Young equation,[40] wettability represents the surface energy which can be obtained by the water contact angle test. Fig. 4 presents the water contact angle of the glass surface as a function of F concentration on the surface. When the F concentration was reduced to 0 (O_2 plasma activation), water droplets spread rapidly on the surface because of the construction of high-density –OH functional groups, and the final contact angle was stabilized at 3°. With the incorporation of sufficient –OH groups, the bonding wave was prone to propagating across the interface even with slight pressure applied with a tweezer. With the addition of F atoms, the contact angle increased significantly and could reach 51° when the F concentration was 11.2%. The relatively hydrophobic glass surface realized *via* (O_2 + F*) plasma was attributed to the electronegativity of F, causing the polar hydrophobicity.[41] However, the room temperature bonding could not be realized with this high concentration, indicating that excessive F atoms had a detrimental effect on bonding.

Considering the effect of fluorination, it is necessary to optimize the F concentration to achieve optimal bonding energy. Without the plasma treatment, the glass substrates were almost impossible to bond, and a fairly weak bonding energy of 0.125 J m^{-2} was obtained, as displayed in Fig. 5(a). Once the surfaces were activated by O_2 plasma, the bonding strength was rapidly improved to 0.6 J m^{-2} after room temperature storage for 48 h, though it was still not robust enough for nanofluidic applications. Subsequently, the optimal F concentration was screened as 5% with the assistance of PTFE, obtaining a maximum bonding energy of 1.534 J m^{-2} with a crack opening length of 10.85 mm, as displayed in Fig. 5(b). In addition, a

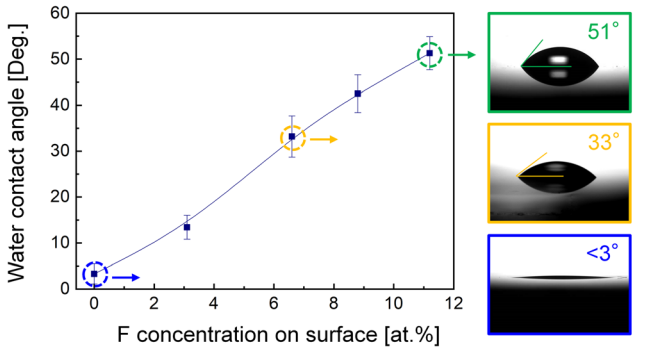

Fig. 4 Hydrophilicity of glass substrates as a function of F concentration on the surface.

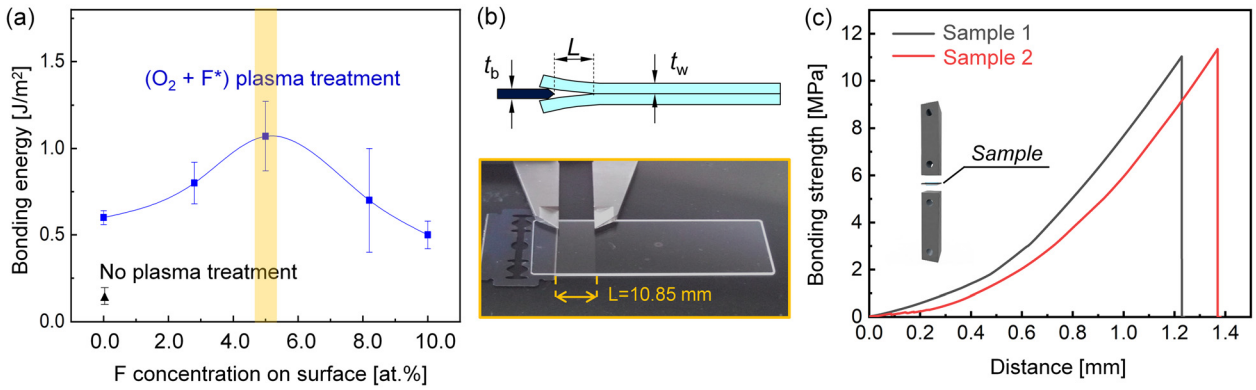

Fig. 5 (a) Evaluation of room-temperature bonding energy with different F concentrations on the surface. The photograph of the crack opening with maximum bonding energy is shown in (b). (c) Tensile strength–distance curve of bonding interface with optimal F concentrations on the surface.

tensile test was also performed for the glass–glass interface with maximum bonding energy. As shown in Fig. 5(c), the room-temperature bonding interface exhibited good bonding strength with a maximum value of 11.3 MPa. However, the further introduction of F atoms could degrade the bonding energy, which was in accordance with the contact angle results. Furthermore, the activated surfaces with optimal F concentrations should be bonded without long-term exposure to preserve surface reactivity. Otherwise, the bonding strength and area would inevitably deteriorate. Fig. S4(a)† presents the bondability of activated surfaces with different air exposure times before bonding in an atmosphere with RH = 75%. Combined with Fig. S4(b),† it can be noted that optimal strength and bonding area could be attained simultaneously *via* timely bonding. However, one can notice that the bonding strength decreased slightly when the functionalized surfaces were bonded within 0.5 h, but still exceeded 8 MPa. With the prolongation of exposure time, the bonding strength was degraded further, and obvious unbonded regions with Newton rings were observed, as depicted in Fig. S4(c).† Ultimately, the surface became completely inactive after 2.5 hours of exposure. Therefore, a maximum storage time of 0.5 h in an atmosphere of RH = 75% was recommended to ensure bonding quality. Similarly, Xu *et al.*[42] introduced F* on glass surfaces *via* a mixture of O_2/CF_4 plasma to obtain an optimal glass–glass bonding energy (1.12 J m^{-2}) at room temperature. However, the flow rate of CF_4 should be precisely controlled at 0.5 sccm *via* accurate gas flow controllers, which are expensive to equip with a commercial plasma chamber. Therefore, it is a more convenient and cost-effective solution to generate F* from PTFE. Moreover, it has been reported that the bonding energy of O_2 plasma-activated Si–Si pairs can be saturated *via* long-term storage like 4000 h,[43] indicating the sufficient occurrence of reaction between the hydroxylated interface. Similarly, it can be speculated that the glass–glass interface obtained by O_2 plasma activation can be further strengthened *via* storage, whereas this duration could be effectively shortened *via* (O_2 + F*) plasma treatment.

Combining the above results, the mechanism of room-temperature bonding *via* PTFE-assisted plasma modification can be illustrated, as shown in Fig. 6. When the glass surface was exposed to O_2 plasma, a sufficiently smooth, hydrophilic surface terminated with sufficient –OH groups was achieved. A hydrogen network could be formed between the hydroxylated glass surfaces with the help of water molecules, determining whether bonding can take place.[44] With increasing temperature or prolonged storage, the weak hydrogen bonds could be converted into strong covalent bonds according to the dehydration reaction (2), which is reversible up to 425 °C.[45] The more by-product H_2O molecules diffused from the interface, the more Si–O–Si covalent bonds were formed, which is more conducive to the strengthening of the interface. Therefore, the interfacial structure had an important influence on the enhancement of bonding energy.

$$Si–OH + HO–Si \rightarrow Si–O–Si + H_2O \quad (2)$$

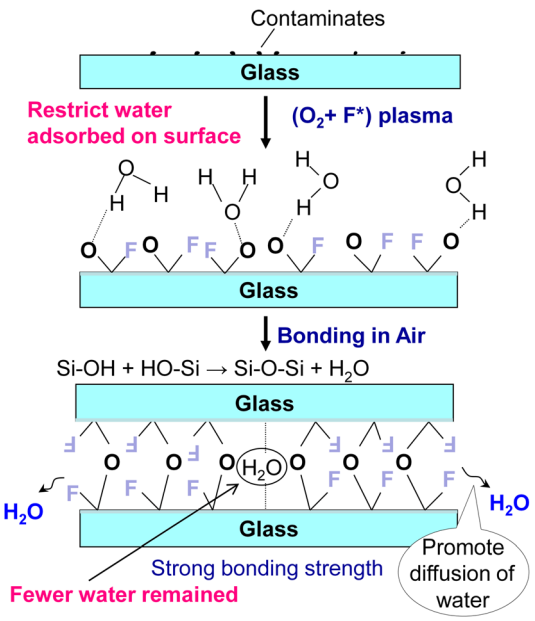

Fig. 6 The mechanism of room-temperature bonding of glass chips *via* PTFE-assisted modification.

Nevertheless, by activating the glass surface with (O_2 + F*) plasma, an outermost surface terminated with Si–OH and Si–F groups and a subsurface structure of SiO_xF_y were obtained. Given the polar hydrophobicity of Si–F groups, the water adsorbed on the plasma-activated surface could be controlled by balancing the amount of –OH and –F groups. Appropriate addition of F could limit the adsorption of H_2O on the surface, whereas excessive hydrophobic groups on the surface could barrier the bonding at room temperature since the hydrogen network cannot be formed with a small number of water molecules.[45] On the other hand, the SiO_xF_y in the subsurface with adequate thickness played a crucial role in facilitating the diffusion of H_2O like a porous "sponge". This is because fluorinated silicon oxide has a lower density than SiO_2 due to its large ring structure.[46,47] Therefore, the establishment of Si–OH and Si–F on the glass surface *via* PTFE modification restricted the adsorption of water molecules initially. After the two glass surfaces came into contact, a hydrogen network was established and the dehydration reactions (2) and (3) occurred at room temperature. Owing to the smaller volume of HF molecules, the diffusion rate of HF in oxides could be much faster than that of H_2O molecules. Subsequently, the SiO_xF_y with a thickness of 2 nm in the subsurface could facilitate the diffusion or dissolution of H_2O and HF at the interface effectively. Eventually, a robust Si–O–Si covalent network was realized by storage for 48 h in ambient air. In addition, we characterized the room-temperature bonding energy of glass–glass as a function of storage time in ambient air, as shown in Fig. S1(b).† One can note that the bonding interface was strengthened significantly and continuously within 24 h. After 24 hours of storage, the interface was shown to be robust enough (>1.0 J m^{-2}) to withstand the post-bonding process such as dicing,[48] illustrating a bonding efficiency comparable to that of sequential plasma activation (24 h).[22] Upon the storage duration exceeding 48 h, the maximum bonding energy was obtained, indicating the sufficient occurrence of dehydration reactions.

$$\text{Si–OH + F–Si} \rightarrow \text{Si–O–Si + HF} \quad (3)$$

Regarding room-temperature bonded glass substrates, there is an urgent need to confirm whether the glass modified *via* PTFE met the requirements for nanofluidic

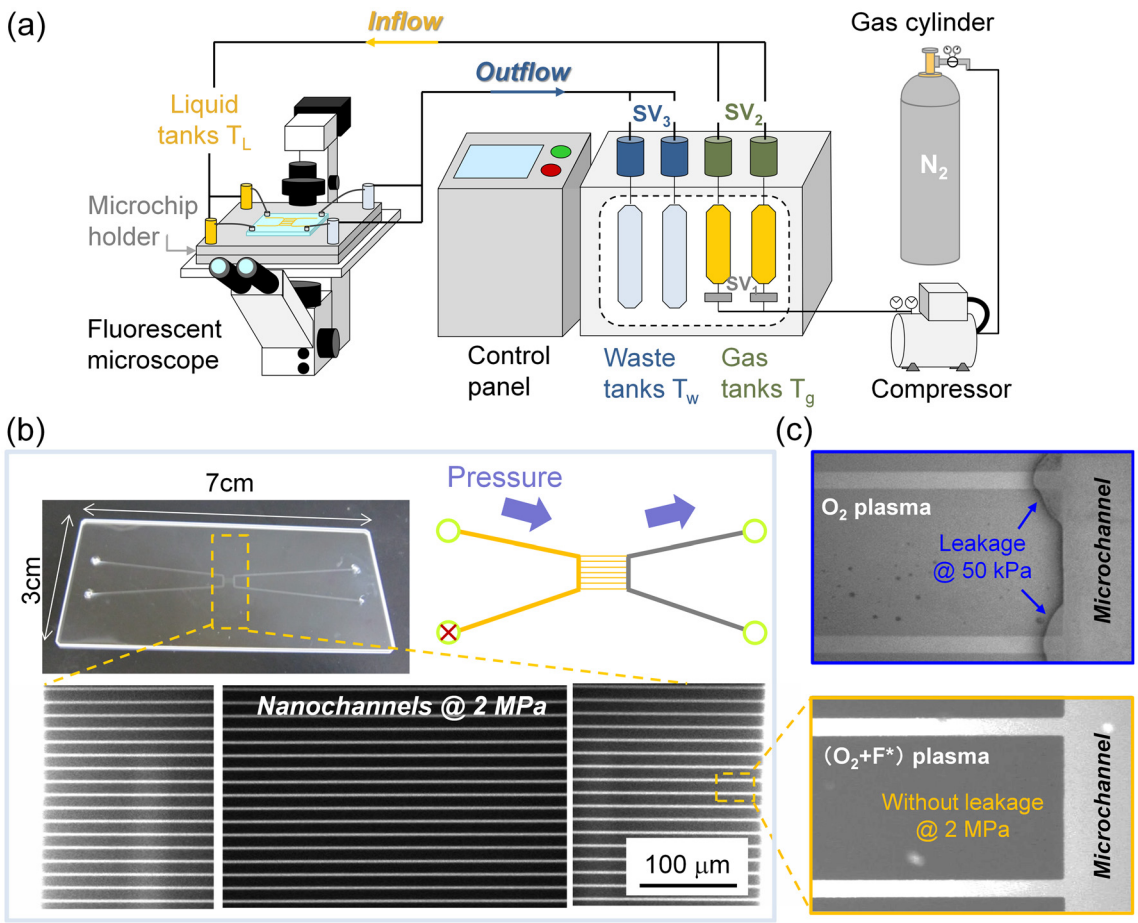

Fig. 7 (a) Schematic illustration of the high-pressure liquid introduction system for the measurement of nanofluidic leakage. (b) The photograph of bonded glass chips with micro and nanochannels and the fluorescence images of nanochannels with the introduction of sulforhodamine B solution. (c) The fluorescence image of the connection of microchannel and nanochannels with different activations.

devices. Thereby, a leakage test was applied to the glass substrates fabricated with micro and nanochannels. Since the nanofluidic channels usually should be able to withstand high pressures of hundreds of kilopascals, here the fluorescent solution was driven into the channels by a self-designed two-channel high-pressure liquid introduction system to verify the bonding strength, which can provide continuous, precise, and higher pressure (50 kPa–2 MPa) required for common nanofluidic applications. As illustrated in Fig. 7(a), N_2 gas was generated from a gas cylinder and the gas pressure was increased up to a maximum of 4.4 MPa using a compressor. The pressurized N_2 gas was divided into two channels and stored in two gas tanks (T_g), and the gas pressure in the T_g could be controlled by the connecting solenoid valves SV_1. Afterward, by opening the solenoid valves SV_2, the sample solution (sulforhodamine B) was pushed from the gas tanks into the connecting liquid tanks (T_L), ready to be introduced into the nanofluidic chip fixed on a stainless steel microchip holder. The connections between the T_L and nanofluidic chip were sealed with Teflon O-rings. It is noteworthy that one of the liquid tanks was filled with sample solutions from the gas tank, while another liquid tank was just filled with pressurized gas to ensure the diffusion of the solution from one side microchannel to the other *via* 20 bridging nanochannels. As sulforhodamine B was driven into the nanofluidic chip, leakage could be observed *via* fluorescence microscopy when the bonding area was filled with fluorescent solution. Eventually, the fluorescent solution could be collected and recycled in waste tanks (T_w) *via* solenoid valves SV_3 to keep the experiment environmentally friendly. The actions of all valves could be controlled through an LCD touch panel.

Based on the abovementioned pressure-driven fluidic control system, Fig. 7(b) shows that sulforhodamine B was introduced into the left side microchannel and center nanochannels (400 nm in width, 200 nm in depth, 700 μm in length), which were sealed by (O_2 + F*) plasma activation at room temperature, and effused from the right side microchannel. Due to the higher Laplace pressure in nanochannels, leakage is more likely to be observed at the nanochannels and connections of the micro and nanochannels. Fig. 7(b) presents that strong fluorescence was observed in all the 700 μm long nanochannels with the continuous introduction of sulforhodamine B at a pressure of 2 MPa, whereas no fluorescence was observed at the bonding interface between the nanochannels, revealing the defect-free interface and sufficient bonding strength. Moreover, as displayed in Fig. 7(c), the enlarged fluorescence image illustrated that a hermetic seal was realized at the connection of the right microchannel and nanochannels, which suggested the successful introduction of the solution into the microchannel *via* bridging nanochannels without leakage. The leak-free glass–glass interface verified the capability of nanofluidic devices assembled *via* (O_2 + F*) plasma to withstand high pressure. In contrast, a fluorescence signal was detected at the connection of the microchannel and nanochannels formed *via* O_2 plasma activation even at a pressure of 50 kPa, indicating the risk of substrate separation under common nanofluidic conditions. Therefore, the stable and robust glass–glass interface fabricated *via* PTFE-assisted plasma modification demonstrated broad prospects for applications spanning sensing, medical diagnostics, high-pressure nanochromatography, *etc.*

In addition, the direct transmittance of bulk substrates and bonded glass pairs was analyzed using a UV-vis spectrophotometer in the wavelength range of 200–800 nm. As presented in Fig. 8, the transmittance of the bulk glass substrate exceeded 93% in the range of 400 nm to 800 nm, indicating the extraordinary optical properties of the glass substrate as a nanofluidic platform. However, the optical transmittance was reduced by less than 1% for the glass pairs bonded at room temperature *via* (O_2 + F*) plasma, exhibiting relatively high transparency which was close to that of the bulk glass substrate. Given the light absorption by the glass itself, it can be concluded that not only was there no defect at the bonding interface, but also the fluorinated SiO_xF_y layer had little effect on the decrease in optical transmittance. Thus, the defect-free bonded glass pairs activated by (O_2 + F*) plasma demonstrated potential for future high-speed, high-sensitivity, and high-resolution optical detection or liquid sensing.

4. Conclusion

In summary, we developed a strong and nano-structure friendly PTFE-assisted plasma modification strategy for glass–glass bonding at room temperature. Because of the cleaning effect, sputtering effect, and chemical reactivity of O_2 plasma, fluorine radicals (F*) were generated from PTFE in a commercialized reactive ion etching plasma chamber, and the glass surface was flattened and functionalized effectively within 40 s. Although the etching effect of fluorine-containing gas on SiO_2 was extensively proved, the addition of trace F* could obtain a smooth glass surface and maintain the profile of precise nanochannels. Without a requirement for immersion in dangerous chemicals such

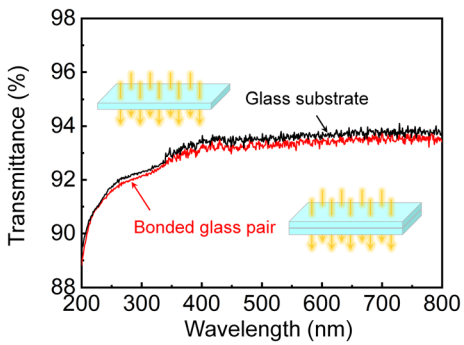

Fig. 8 UV-vis transmission spectra of the bulk glass (700 μm thick) and the glass/glass bonded pair (1400 μm thick in total).

as HF, a Si–OH and Si–F terminated glass surface with fluorinated silica oxide in the subsurface was obtained *via* the (O_2 + F*) plasma treatment, and this fluorinated SiO_xF_y layer had little effect on the light transmittance. By controlling the F concentration on the surface, a maximum bonding energy of 1.534 J m^{-2} was achieved after room-temperature storage for 48 h, which was almost three times stronger than that of the interface realized by only O_2 plasma activation. Moreover, the capability of this PTFE-assisted plasma modification strategy for nanofluidic devices was verified, and a leak-free glass–glass interface with high-pressure resistance (2 MPa) would exhibit great potential for applications immobilized by temperature-sensitive functional components.

Conflicts of interest

There are no conflicts to declare.

Acknowledgements

This work was financially supported by the National Natural Science Foundation of China (Grant No. 51975151 and 92164105), the Heilongjiang Provincial Natural Science Foundation of China under grant LH2019E041, and the Heilongjiang Touyan Innovation Team Program (HITTY-20190013). The authors also acknowledge financial support from the Core Research for Evolutional Science and Technology (CREST) program of the Japan Science and Technology (JST) *via* grant no. JPMJCR14G1.

References

1 D. R. Reyes, D. Iossifidis, P. Auroux and A. Manz, *Anal. Chem.*, 2002, **74**, 2623–2636.
2 D. Najjar, J. Rainbow, S. Sharma Timilsina, P. Jolly, H. de Puig, M. Yafia, N. Durr, H. Sallum, G. Alter, J. Z. Li, X. G. Yu, D. R. Walt, J. A. Paradiso, P. Estrela, J. J. Collins and D. E. Ingber, *Nat. Biomed. Eng.*, 2022, **6**, 968–978.
3 M. Yafia, O. Ymbern, A. O. Olanrewaju, A. Parandakh, A. Sohrabi Kashani, J. Renault, Z. Jin, G. Kim, A. Ng and D. Juncker, *Nature*, 2022, **605**, 464–469.
4 H. Hisamoto, Y. Shimizu, K. Uchiyama, M. Tokeshi, Y. Kikutani, A. Hibara and T. Kitamori, *Anal. Chem.*, 2003, **75**, 350–354.
5 H. Hisamoto, T. Saito, M. Tokeshi, A. Hibara and T. Kitamori, *Chem. Commun.*, 2001, 2662–2663.
6 S. I. Funano, N. Ota and Y. Tanaka, *Lab Chip*, 2021, **21**, 2244–2254.
7 Y. Xu, C. Wang, Y. Dong, L. Li, K. Jang, K. Mawatari, T. Suga and T. Kitamori, *Anal. Bioanal. Chem.*, 2012, **402**, 1011–1018.
8 D. I. Rozkiewicz, B. J. Ravoo and D. N. Reinhoudt, *Supramol. Chem. Org.–Inorg. Hybrid Mater.*, 2010, 433–466.
9 Y. Ding, S. Garland, M. Howland, A. Revzin and T. Pan, *Adv. Mater.*, 2011, **23**, 5551–5556.
10 B. Samel, M. K. Chowdhury and G. Stemme, *J. Micromech. Microeng.*, 2007, **17**, 1710–1714.
11 L. Yu, F. E. H. Tay, G. Xu, B. Chen, M. Avram and C. Iliescu, *J. Phys.: Conf. Ser.*, 2006, **34**, 776–781.
12 X. Zhou, S. Virasawmy and C. Quan, *Microsyst. Technol.*, 2009, **15**, 573–580.
13 J. Q. Lu, J. J. McMahon and R. J. Gutmann, *Mater. Res. Soc. Symp. Proc.*, 2009, **1112**, 69–80.
14 N. Y. Lee and B. H. Chung, *Langmuir*, 2009, **25**, 3861–3866.
15 V. Sunkara and Y. K. Cho, *ACS Appl. Mater. Interfaces*, 2012, **4**, 6537–6544.
16 J. Xu, C. Wang, S. Zhou, R. Zhang and Y. Tian, *Ceram. Int.*, 2019, **45**, 16670–16675.
17 M. Zhang, J. Zhao and L. Gao, *Sens. Actuators, A*, 2008, **141**, 213–216.
18 L. Tang and N. Y. Lee, *Lab Chip*, 2010, **10**, 1274–1280.
19 J. Bart, R. Tiggelaar, M. Yang, S. Schlautmann, H. Zuilhof and H. Gardeniers, *Lab Chip*, 2009, **9**, 3481–3488.
20 M. Iwakura, D. Nakamura, T. Takenawa and Y. Mitsuishi, *Protein Eng.*, 2001, **14**, 583–589.
21 B. Renberg, K. Sato, K. Mawatari, N. Idota, T. Tsukahara and T. Kitamori, *Lab Chip*, 2009, **9**, 1517–1523.
22 M. M. R. Howlader, S. Suehara and T. Suga, *Sens. Actuators, A*, 2006, **127**, 31–36.
23 K. Takeuchi, F. Mu, Y. Matsumoto and T. Suga, *Adv. Mater. Interfaces*, 2021, **8**, 1–8.
24 Z. J. Jia, Q. Fang and Z. L. Fang, *Anal. Chem.*, 2004, **76**, 5597–5602.
25 H. Nakanishi, T. Nishimoto, M. Kanai, T. Saitoh, R. Nakamura, T. Yoshida and S. Shoji, *Sens. Actuators, A*, 2000, **83**, 136–141.
26 L. Chen, G. Luo, K. Liu, J. Ma, B. Yao, Y. Yan and Y. Wang, *Sens. Actuators, B*, 2006, **119**, 335–344.
27 Y. Wang, Y. Xu, S. Dong, P. Wang, W. Chen, Z. Lu, D. Ye, B. Pan, D. Wu, C. D. Vecitis and G. Gao, *Nat. Commun.*, 2021, **12**, 1–8.
28 G. Primc, *Polymer*, 2020, **12**, 1–7.
29 W. P. Maszara, G. Goetz, A. Caviglia and J. B. McKitterick, *J. Appl. Phys.*, 1988, **64**, 4943–4950.
30 F. Persson, J. Fritzsche, K. U. Mir, M. Modesti, F. Westerlund and J. O. Tegenfeldt, *Nano Lett.*, 2012, **12**, 2260–2265.
31 K. Morikawa, K. Mawatari, M. Kato, T. Tsukahara and T. Kitamori, *Lab Chip*, 2010, **10**, 871–875.
32 Y. Xu and B. Xu, *Small*, 2015, **11**, 6165–6171.
33 T. Tsukahara, K. Mawatari, A. Hibara and T. Kitamori, *Anal. Bioanal. Chem.*, 2008, **391**, 2745–2752.
34 W. Xu, E. Foster, C. Ma and P. W. Bohn, *Microfluid. Nanofluid.*, 2015, **19**, 1181–1189.
35 Y. Xu, M. Shinomiya and A. Harada, *Adv. Mater.*, 2016, **28**, 2209–2216.
36 A. Kaur, P. Chahal and T. Hogan, *IEEE Electron Device Lett.*, 2016, **37**, 142–145.
37 C. Wang and T. Suga, *ECS J. Solid State Sci. Technol.*, 2016, **5**, P393–P395.
38 J. A. Colony and E. L. Sanford, Nasa Tm/100681, 1987, p. 10.
39 D. J. Oostra, *J. Vac. Sci. Technol., B: Microelectron. Process. Phenom.*, 1986, **4**, 1278.

40 M. A. Miranda, A. Ghosh, G. Mahmodi, S. Xie, M. Shaw, S. Kim, M. J. Krzmarzick, D. J. Lampert and C. P. Aichele, *Water*, 2022, **14**, 880.
41 S. Roy, B. Biswas, N. Ghosh, P. C. Singh and J. A. Mondal, *J. Phys. Chem. C*, 2019, **123**, 27012–27019.
42 Y. Xu, C. Wang, L. Li, N. Matsumoto, K. Jang, Y. Dong, K. Mawatari, T. Suga and T. Kitamori, *Lab Chip*, 2013, **13**, 1048–1052.
43 T. Plach, K. Hingerl, S. Tollabimazraehno, G. Hesser, V. Dragoi and M. Wimplinger, *J. Appl. Phys.*, 2013, **113**, 094905.
44 Q. Y. Tong and U. M. Gösele, *Adv. Mater.*, 1999, **11**, 1409–1425.
45 Q. Y. Tong and U. M. Gösele, *Semiconductor Wafer Bonding: Science and Technology*, Wiley, New York, 1999.
46 A. Kazor, C. Jeynes and I. W. Boyd, *Appl. Phys. Lett.*, 1994, **65**, 1572–1574.
47 V. Pankov, J. C. Alonso and A. Ortiz, *J. Appl. Phys.*, 1999, **86**, 275–280.
48 H. Takagi, Y. Kurashima, A. Takamizawa, T. Ikegami and S. Yanagimachi, *Jpn. J. Appl. Phys.*, 2017, **57**, 02BA04.